Contrib Mineral Petrol (2002) 144: 109–127
DOI 10.1007/s00410-002-0388-z

Ralf Halama · Tod Waight · Gregor Markl

Geochemical and isotopic zoning patterns of plagioclase megacrysts in gabbroic dykes from the Gardar Province, South Greenland: implications for crystallisation processes in anorthositic magmas

Received: 2 May 2002 / Accepted: 14 June 2002 / Published online: 22 August 2002

Abstract Chemical and Sr isotopic zoning patterns in plagioclase megacrysts from gabbroic dykes in the Gardar Province can be used to elucidate magma-chamber and emplacement processes. The megacrysts occur either as single crystals or assembled as anorthosite xenoliths. The size of the megacrysts varies from <1 cm to 1 m. They consist of a large core with variable zonation ($An_{58–39}$) and a relatively small (<600 μm), normally zoned rim ($An_{62–27}$). The contact between core and rim is sharp and marked by a sharp increase in anorthite content which can reach 11 mol% An. This gap is interpreted as having formed during dyke emplacement due to a sudden pressure release. Some of the megacryst cores show a fairly constant composition whereas others exhibit an unusual wavy-oscillatory zoning which has not been reported elsewhere to our knowledge. The oscillatory zoning has wavelengths of up to 2,500 μm and a maximum amplitude of 7 mol% An. It is interpreted as reflecting movements of the crystals in the magma reservoir. The Sr isotopic composition of one crystal shows a radiogenic inner core ($(^{87}Sr/^{86}Sr)_i = 0.7044$) and a less radiogenic outer core ($(^{87}Sr/^{86}Sr)_i = 0.7039–0.7036$). The lack of a significant change between outer core and rim ($(^{87}Sr/^{86}Sr)_i = 0.7037$) is consistent with formation of the more An-rich rim due to pressure release. Variations in the core may be related to movements of the crystal and/or magma mixing. A trace-element profile across a megacryst shows a small increase in Sr and small decreases in Ba and La contents of the recalculated melt composition across the core-rim boundary, whereas P, Ce, Nd and Eu remain constant. Melt compositional changes upon emplacement are therefore considered to be of minor importance. Constant ratios of incompatible trace elements in the megacryst cores indicate a dominant influence of a lower crustal source on trace-element budgets.

R. Halama · G. Markl (✉)
Institut für Geowissenschaften,
Eberhard-Karls-Universität Tübingen,
Wilhelmstr. 56, 72074 Tübingen, Germany
E-mail: markl@uni-tuebingen.de
Tel.: +49-7071-2972930
Fax: +49-7071-293060

T. Waight
Danish Lithosphere Centre, Øster Voldgade 10 L,
1350 Copenhagen, Denmark

Editorial responsibility: J. Hoefs

Introduction

Massif-type anorthosites (MTAs) are large intrusive bodies (up to 17,000 km^2) mainly restricted to the middle Proterozoic (1.6–1.1 Ga) and which contain vast accumulations of plagioclase ($An_{50\pm10}$) with subordinate mafic minerals (Ashwal 1993 and references therein). They represent the most voluminous anorthosite type on Earth and their relatively sodic plagioclase makes them distinct from other anorthositic rocks (Ashwal 1993). Various mechanisms have been proposed to explain the presence of such plagioclase-rich rocks, including the formation of plagioclase cumulates from basaltic magmas (e.g. Morse 1982), resorption and remelting of plagioclase (Wiebe 1990), delayed nucleation of plagioclase in mafic melts with the formation of "hyperfeldspathic" liquids (Morse 1982), and interaction between aluminous crust and basaltic magma (e.g. Dempster et al. 1999). The composition of the melts parental to anorthosites is thought to be broadly basaltic (e.g. Bowen 1917; Emslie 1978; Scoates 2000) or jotunitic (e.g. Vander Auwera et al. 1998; Owens and Dymek 2001) but these melt compositions are usually not preserved due to crystal fractionation and accumulation processes.

The ultimate source of the magmas from which the anorthosites crystallised is still much debated, with two principal schools of thought: magmas sourced (1) from the mantle (e.g. Emslie 1978; Wiebe 1992; Mitchell et al. 1995; Markl and Frost 1999) or (2) from the lower crust (e.g. Longhi et al. 1999; Schiellerup et al. 2000; Bédard 2001). Most authors believe in some sort of interaction

between mantle-derived and crustal material during anorthosite genesis, via either crustal contamination of mantle-derived magmas (e.g. Scoates and Frost 1996) or contamination of remobilised crust by basalt (Bédard 2001).

In the Gardar Province, gabbroic "Big Feldspar Dykes" (BFDs) contain both numerous, single plagioclase megacrysts and anorthosite xenoliths, and are interpreted to record the formation of anorthositic bodies at depth (Bridgwater 1967; Bridgwater and Harry 1968). Bridgwater (1967) has shown that the feldspathic material in the dykes is genetically linked to the present host, although it did not crystallise in place. Since the Precambrian of Greenland is a continuation of the Canadian Shield, with similar tectonic divisions and orogenic activities at approximately the same time, a close link between the Gardar anorthosite inclusions and the MTAs of the Canadian Shield has been postulated (Bridgwater 1967). The fact that emplacement ages of the Gardar dykes (~1.15–1.25 Ma) overlap with ages obtained for Canadian anorthosites (e.g. Higgins and van Breemen 1992; Owens et al. 1994) further suggests a genetic relationship between the provinces. Additionally, the Gardar feldspathic material has X_{An} values within the range typical of plagioclase from these anorthosite massifs.

For the Canadian anorthosites, pressure estimates, assumed to represent the final level of emplacement, vary from 3 to 5 kbar (Fuhrmann et al. 1988; Kolker and Lindsley 1989) whereas the Gardar rocks show emplacement depths of 3–4 km corresponding to a pressure of ~1 kbar, based on fluid-inclusion data from Ilímaussaq (Konnerup-Madsen and Rose-Hansen 1984). The Gardar dykes with their numerous feldspathic inclusions most likely represent a higher level of exposure of an anorthosite province which is similar to, or even the continuation of, the Canadian Shield. Therefore, a study of the BFDs offers a unique opportunity to reveal details and independent constraints on magma-chamber and emplacement processes at depth during anorthosite genesis.

Examining the "Big Feldspar Dykes" as whole rocks is not useful in the present context because the rocks contain variable amounts of plagioclase megacrysts and do not represent true liquids. Single crystals, however, should preserve information on magma compositions and processes during anorthosite genesis. Investigations on single feldspar crystals have been very successful in elucidating the temporal record of magma-chamber dynamics (e.g. Singer et al. 1995; Tepley et al. 1999) and the liquidus chemistry of magmas (e.g. Blundy and Wood 1991; Bindeman et al. 1999). Due to the very low diffusivities of major- and trace-element cations (Giletti 1994; Giletti and Shanahan 1997) and high closure temperatures (Cherniak and Watson 1992; Cherniak 1995) in plagioclase, it can be assumed that plagioclase preserves its original composition during cooling, down to a scale of micrometres. Compositional and textural zoning should reflect processes during growth because the diffusive exchange CaAl – NaSi in plagioclase is slow (Grove et al. 1984).

Based on major- and trace-element compositional zoning and/or Sr and Nd isotopic zoning in feldspar, evidence for magma recharge (e.g. Tepley et al. 2000; Davidson et al. 2001), assimilation (e.g. Knesel et al. 1999), magma mixing and mingling (Waight et al. 2000, 2001), convection (Loomis and Welber 1982) and fractional crystallisation processes (Brophy et al. 1996) has been presented in different contexts. Many of those studies concentrated on silicic volcanic and plutonic rocks or on the interplay between the respective magmas, but few dealt with basaltic systems (e.g. Pringle et al. 1974; Kuritani 1998; Bindeman et al. 1999) or anorthositic rocks (e.g. Wiebe 1992).

The present study investigates chemical and isotopic zoning in single plagioclase megacrysts from two BFDs of the Gardar Province which have the potential to constrain certain aspects of parental-melt compositions and to provide information about dynamics and processes recorded within an anorthositic magma chamber.

Geological background

The Gardar Province of South Greenland represents a mid-Proterozoic rift province with abundant alkaline magmatism lasting from about 1.30 to 1.12 Ga (Emeleus and Upton 1976; Upton and Emeleus 1987). It encompasses about ten igneous complexes, numerous dykes of variable chemical composition, and a sequence of interlayered lavas and sediments (Eriksfjord Formation). During the late Gardar period (~1.20–1.12 Ga), several generations of gabbroic and intermediate dykes were emplaced along WSW–ENE to SW–NE trends, concentrated in two main zones (Upton and Emeleus 1987). The emplacement time of the more northerly Nunarssuit-Isortoq swarm is poorly constrained but demonstrably younger than 1,250 Ma (Patchett et al. 1978) and post-dating the early "brown dykes" (BD_0s) dated at $1{,}282 \pm 5$ Ma (Upton, personal communication). The swarm pre-dates the Nunarssuit syenite for which a U/Pb date is $1{,}171 \pm 5$ Ma (Finch et al. 2001). This is confirmed by a Sm–Nd cpx–plag whole-rock isochron for a dyke from this region which yielded an age of $1{,}190 \pm 44$ Ma (Halama, unpublished data). Many of the dykes contain abundant anorthosite xenoliths and plagioclase megacrysts and are therefore informally named "Big Feldspar Dykes". The feldspathic material is considered as evidence for an anorthosite body underlying South Greenland (Bridgwater 1967). The megacrysts are interpreted to have formed as unconsolidated roof material in a magma chamber, either as free-floating suspended crystals or derived from overlying anorthosite (Bridgwater and Harry 1968). Large, euhedral crystals have never accumulated to form solid anorthosite. They represent an end member in a continuous textural series from single plagioclase crystals to massive plagioclase rock. Bridgwater (1967) emphasised the genetic

connection between host rocks and inclusions and inferred that the megacrysts are not true xenocrysts. The basic magmas which carried up the megacrysts were evolved magmas with low Ni contents, low Mg# and high Al/Ca ratios (Upton 1996).

Since the Gardar Province has been tectonically quiet after magmatic activity ceased and no metamorphic events affected the rocks, it is well suited for a study on magmatic processes based on mineral textures and analyses of primary magmatic phases.

Field observations and petrography

Ubiquitous gabbroic "Big Feldspar Dykes" occur in the Isortoq region in the western part of the Gardar Province (Fig. 1). They belong to the Nunarssuit-Isortoq dyke swarm which covers an area of roughly 50×25 km, and they were emplaced into granitic basement of the Proterozoic Ketilidian mobile belt (Allaart 1976). The BFDs vary in width from a few metres to 100 m. A detailed account of the field relationships has been given by Bridgwater and Harry (1968).

The major matrix mineral phases of the gabbroic BFDs are plagioclase, olivine, clinopyroxene and titanomagnetite. Minor phases are apatite and biotite; pyrrhotite, chalcopyrite, sphalerite and baddeleyite occur as accessory minerals. Additionally, amphibole has been found in the anorthosite xenolith sample. Euhedral matrix plagioclase (width < 300 μm) is normally zoned and represents an early liquidus phase, followed by olivine and clinopyroxene. Biotite occurs either as fringes around Fe–Ti oxides or as euhedral grains.

The characteristic feature of the BFDs is their high content of feldspathic material, varying from single feldspar crystals (< 1 cm to 1 m in size) to anorthositic bodies up to 30 m long (Fig. 2). These bodies may vary in composition from leucogabbroic to anorthositic and are not true xenoliths, but the term "anorthosite xenolith" is maintained here to remain consistent with previous publications. The boundary between feldspathic inclusions and a megacryst-free dyke matrix can be relatively sharp or gradual with a continuous decrease in feldspar megacryst concentration towards the matrix (Fig. 3a, b). The distribution of megacrysts within the BFDs is mostly random but at some localities the plagioclase megacrysts are concentrated at the dyke centres (Fig. 3c). The distribution of plagioclase megacrysts can vary within a single dyke and from dyke to dyke. Occasionally, xenoliths of granitic wall rock up to several dm in size can be found in the dykes close to their margins.

Several megacrysts from two different BFDs have been investigated in this study. BFD 1 is on average 50–70 m wide and samples were taken from locations distributed over a length of ~8 km (Fig. 1). With the notable exception of the anorthosite xenolith sample GM 1682, the dyke matrix is olivine-bearing and quartz-free. Samples from BFD 2 were taken from a 12-m-wide dyke section at the shoreline. The matrix of BFD 2 is olivine-free and contains late interstitial quartz.

Analytical methods

Electron microprobe measurements

Mineral compositions were determined using a JEOL 8900 electron microprobe at the Earth Science Department at the University of Tübingen, Germany. An internal $\varphi\rho Z$ correction of the raw data was applied (Armstrong 1991). Both natural and synthetic standards were used for major and minor elements. Measuring times were 16 and 30 s on the peak positions for major and minor elements respectively. The emission current was 15 nA and the acceleration voltage 15 kV. For all feldspar analyses, a beam diameter of 5 μm was used to avoid errors resulting from diffusion of Na.

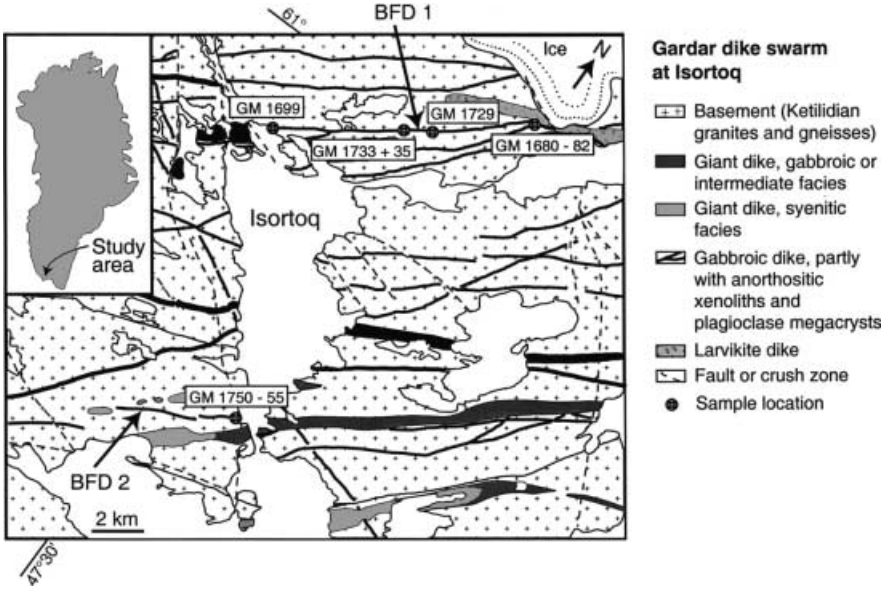

Fig. 1. Geological map of the Isortoq region after Bridgwater and Coe (1970)

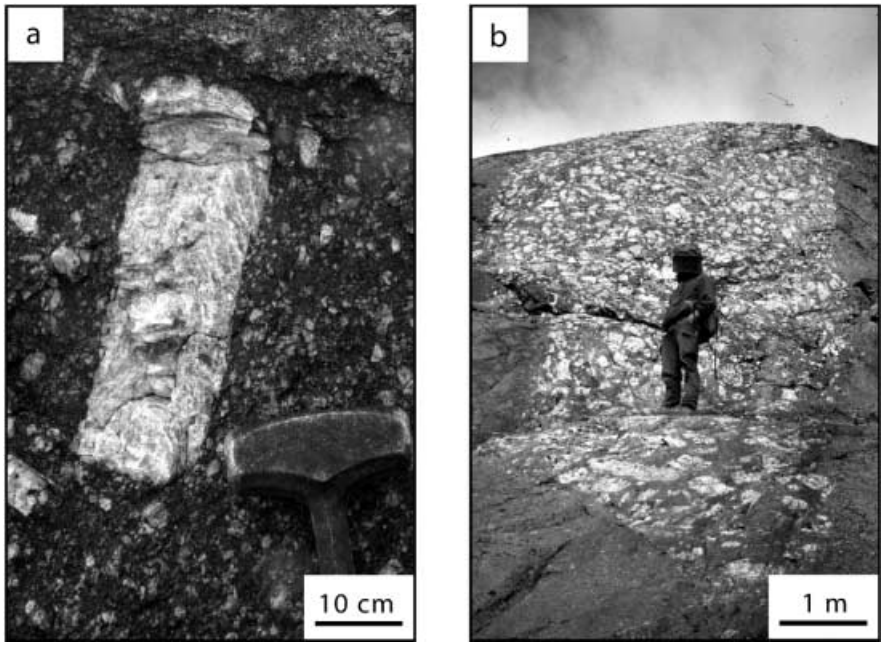

Fig. 2a, b. Occurrences of feldspathic inclusions in the "Big Feldspar Dykes" of Isortoq. **a** Euhedral feldspar megacryst, length about 40 cm. **b** Anorthositic xenolith in fine-grained dyke matrix, total length of xenolith about 20 m

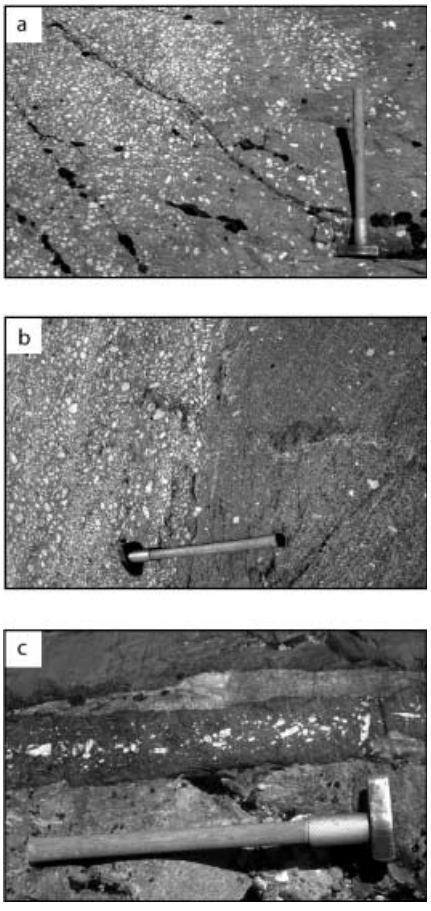

Fig. 3a–c. Field relationships between feldspathic inclusions and dykes (length of hammer 60 cm). **a** Gradual transition from feldspar-rich zone to relatively feldspar-poor host dyke matrix. **b** Sharp contact between feldspar-rich and feldspar-poor areas of the dyke. **c** Small dyke showing a concentration of feldspar megacrysts in the dyke centre. Dyke margins are virtually megacryst-free

Strontium isotope measurements

Drilled feldspar samples for Sr isotopic analyses were collected from polished mineral surfaces using diamond-coated dentist drills with variable diameters (< 1 mm) and methods described by Waight et al. (2000). The small amounts of feldspar powder from the shallow drill pits (< < 1 mm) were collected as a slurry, then dried and weighed to determine sample weight. Samples were spiked with an enriched ^{84}Sr–^{87}Rb mixed tracer and then dissolved in small amounts of HF, HNO_3 and HCl. Rb and Sr were separated using a single pass over a small bed of AG50-X12 resin with HCl elution, followed by cleanup of both the Rb and Sr cuts using Sr-specific resin. Sr isotopic values were determined using a VG Axiom MC-ICPMS at the Danish Lithosphere Centre, Copenhagen. Sample introduction was carried out using a Micromist nebuliser with Ar as both carrier and nebuliser gas. Mass fractionation during the Rb analyses was monitored using admixed Zr, and during the Sr runs it was corrected using $^{84}Sr/^{86}Sr = 0.1194$. Further details of analytical procedures are outlined in Waight et al. (2002). Analyses of SRM 987 over the period of this study gave $^{87}Sr/^{86}Sr = 0.71025 \pm 3$ (2 S.D., $n = 5$). Errors for Sr drill samples are assumed to be $\pm 0.015\%$ which is slightly higher than the precision for whole-rock samples due to difficulties in obtaining an accurate sample weight on such small samples because of static charge effects on Teflon beakers. However, errors in elemental concentrations do not affect elemental ratios and $^{87}Rb/^{86}Sr$ ratios are expected to be correct within 0.5%. All initial Sr isotopic ratios have been corrected for radiogenic growth to an age of 1.19 Ga – the emplacement age of the dyke (Halama, unpublished data) – using $\lambda = 1.42*10^{-11}$ a^{-1} (Steiger and Jäger 1977). Despite the possibility that the megacrysts may have grown earlier and the uncertainty in the age determination (error of ± 44 Ma), errors in age correction are insignificant due to the very low Rb/Sr ratios in all samples except the rim sample, which has larger errors due to a higher Rb content coupled with smaller sample size (see below). However, extrapolation of age errors for this sample results in a calculated error of 0.70371 ± 18 which does not affect the conclusions of this study.

Trace-element measurements

In-situ laser ablation-inductively coupled plasma-mass spectrometer (LA-ICP-MS) trace-element analyses were performed at the EU Large-Scale Geochemical Facility (University of Bristol) using a VG Elemental PlasmaQuad 3 + S-Option ICP-MS equipped with

a 266-nm Nd-YAG laser (VG MicroProbe II). The laser beam diameter at the sample surface was approximately 20 μm for all analyses, and the laser repetition rate was 6 Hz. Helium gas and then an argon/helium mixture carried the ablated material from the sample cell to the plasma torch. All measurements were made using Thermo Elemental PlasmaLab "time-resolved analysis" (TRA) data acquisition software with a total acquisition time of 100 s per analysis, allowing about 40 s for background followed by 50 s for laser ablation. NIST 610 glass was used for instrument calibration, and NIST 612 was used as a secondary standard. Ca was used as an internal standard to correct the ablation yield differences between and during individual analyses on both standards and samples. To avoid analytical uncertainties due to variations in the concentrations of the internal standard, Ca concentrations were quantitatively measured within 20 μm of the laser ablation pits using a JEOL 8900 electron microprobe (EMP) at Tübingen University (see above). The precision of trace-element concentrations, based on replicate analyses of standards, is approximately ±5% for element concentrations >10 ppm, and ±10% for concentrations <10 ppm. Data processing was carried out offline by means of the same PlasmaLab software used for data collection and various custom-designed Excel spreadsheets. The limits of detection are defined as 3.28 standard deviations above the background level, which equates to a 95% confidence that the measured signal is significantly above background. Typical detection limits during this study were 0.1–1 ppm for Sr, Y, Sn, Pb and REEs, 0.5–10 ppm for V, Zn, Ga, Ge, Rb, Cs and Ba, and >10 ppm for P.

Results

Major-element zoning in plagioclase

The chemical inter-crystal variation of 14 plagioclase megacrysts and of matrix plagioclase from two BFDs has been studied. The most distinctive features of matrix plagioclases compared to megacrysts is their strong normal zoning ($An_{62–27}$) and their considerably smaller grain size (widths generally <300 μm). Most megacrysts consist of a homogeneous or weakly oscillatory zoned core which dominates the crystal, and a relatively narrow (<600 μm), normally zoned rim (Figs. 4, 5). Four crystals with several distinctive features will be described in detail, followed by a comparison of the various megacrysts within a single dyke and observed differences between the two dykes. Representative microprobe analyses of both megacrysts and matrix plagioclase are presented in Table 1.

GM 1680, f 6 (BFD 1; width ~8 mm)

This sample contains only a few megacrysts in a medium-grained matrix. The core of the investigated megacryst (f 6) shows a true but weak oscillatory pattern for both An and Ab contents (Fig. 4a). The amplitude between the An peak at 750 μm (X_{An}~50.5) and the An trough at 1,950 μm (X_{An}~46.5) is roughly 4 mol% An. Although a complete period is cut short by the rim growth, $\lambda/2$ can be determined to be 1,200 μm and a wavelength λ of 2,400–2,500 μm is indicated. The Or content stays constant at about 2.5 to 3.5 mol% throughout the core and does not show any oscillatory zoning. The sharp increase in An content at the core-rim boundary amounts to 11 mol%, which is the highest in all crystals studied. The boundary between core and rim is highly irregular, with many areas of An-rich composition within the core and apparent remnants of core composition within the rim zone (Fig. 6). In addition, an alignment of small inclusions (<100 μm) occurs in the core-rim boundary zone. These inclusions consist of clinoamphibole, clinopyroxene, K-feldspar and titanite. The normal zoning trend in the rim, from An_{62} to An_{53}, is smoothly continuous at the beginning but then passes over into a fine-scale oscillatory pattern with amplitudes of several mol% An. The Or content in the rim is significantly lower than in the core, on average about 1.4 mol% Or.

Fig. 4a, b. Microprobe profiles through two plagioclase megacrysts with wavy-oscillatory pattern and normally zoned rims. **a** Wavy-oscillatory pattern throughout the core of the megacryst, followed by a sharp increase in X_{An} at the rim. **b** Initially constant X_{An}, followed by a wavy-oscillatory pattern and a sharp increase in X_{An} at the rim

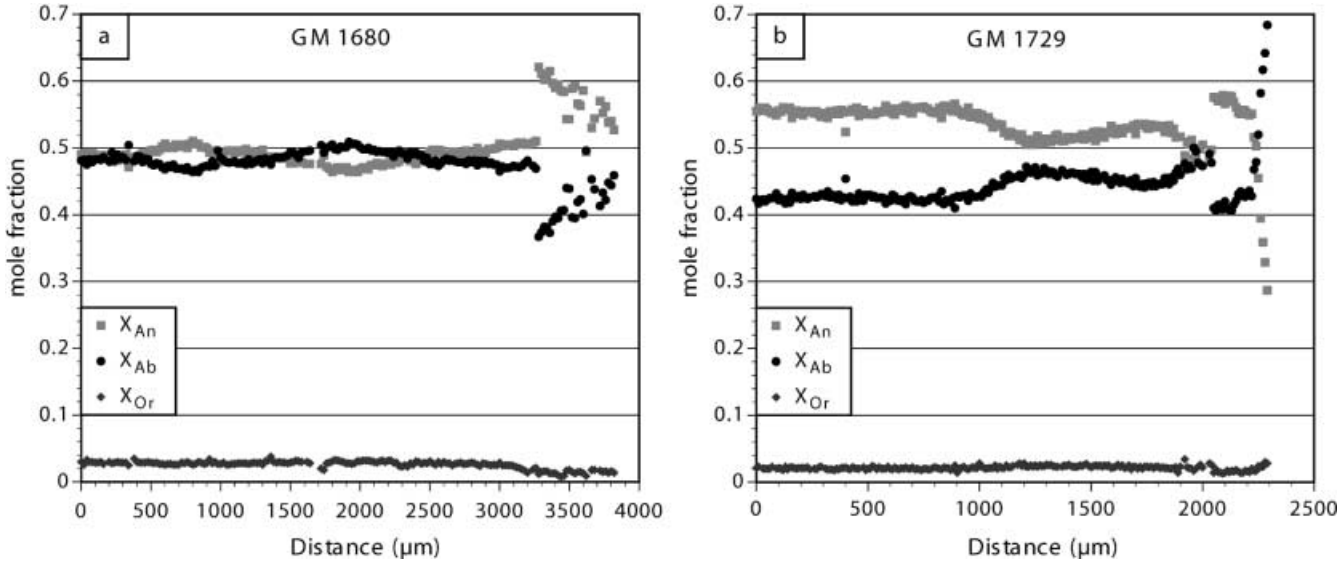

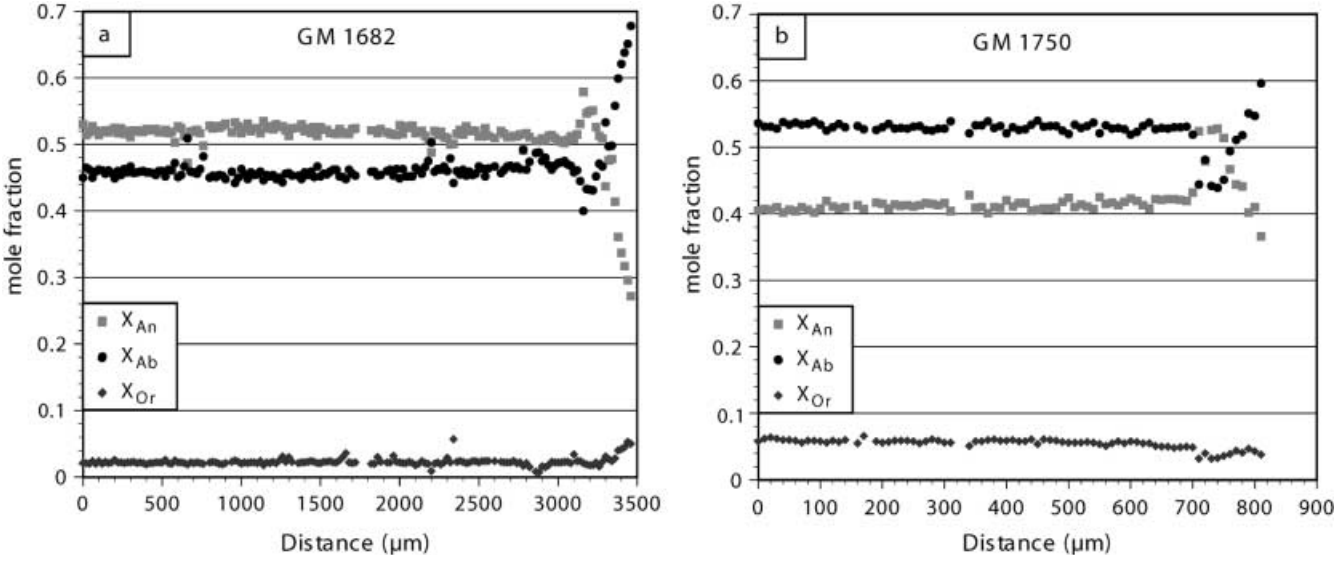

Fig. 5a, b. Microprobe profiles through two plagioclase megacrysts with constant X_{An} in the core and normally zoned rims. **a** X_{An} shows a slight tendency to decrease towards the rim and increases smoothly at the core-rim boundary, before dropping almost 30 mol% in the rim. **b** Within the core, X_{An} has a slight tendency to increase towards the rim before increasing sharply at the core-rim boundary. X_{An} shows normal zoning in the rim

GM 1729, f 4 (BFD 1; width ~4 mm)

In this sample, plagioclase megacrysts of variable size make up 20–40% of the rock volume. In megacryst f 4, the An content remains relatively constant at approximately $An_{56\pm1}$ for the first 900 μm (Fig. 4b). X_{An} oscillates slightly over the next 1,100 μm, matched by variations in Ab content. $\lambda/2$ within this period of growth is ~500 μm, less than half the value of 1,200 μm estimated for GM 1680. The crystal rim is marked by a sharp An increase of 8 mol%, combined with a decrease in Or content of roughly 1 mol%. X_{An} decreases smoothly in the inner rim, but drops sharply in the outer 80 μm to An_{29}. Once the An content has dropped below 50 mol%, the Or content increases from ~1.5 to ~3 mol%. In the core, however, Or content remains constant despite the large variations in An content.

GM 1682, f 3 (BFD 1; width ~11 mm)

This sample was taken from the large anorthosite xenolith shown in Fig. 2b. The remarkably constant core composition of $An_{51\pm1}$ is interrupted by only a few outliers which are probably related to alteration along cracks and/or small inclusions. The core-rim boundary is different from those of the two crystals described above (Fig. 5a) – the increase in An content is more continuous and less pronounced ($\Delta An = 5$ mol%), and a significant drop in Or content is lacking. In the rim, the decrease of X_{An} is relatively steep from An_{58} to An_{27}.

GM 1750, f 1 (BFD 2; width ~3 mm)

This sample is similar to GM 1729, with plagioclase megacrysts of variable size in a fine- to medium-grained matrix. The core composition of crystal f 1 is very constant with An content $\sim41\pm1$ and Or content $\sim6\pm1$ (Fig. 5b). ΔAn at the core-rim boundary is 9 mol% (jumping from An_{43} to An_{52}), with Or content dropping about 2 mol% from 5 to 3. The rim initially has a composition at about An_{52}, followed by a decrease to An_{37}.

The matrix plagioclases of samples GM 1680, GM 1729 and GM 1750 are all normally zoned and show a variation in X_{An} similar to that observed in megacryst rims. However, the highest An content in the matrix plagioclases is usually slightly less than the highest An content in the megacryst rims (Table 2).

To investigate similarities and differences between plagioclase megacrysts within a single dyke and between the two dykes, the average An content of the megacryst core region was calculated and plotted against the maximum An content in the core (Fig. 7). As expected, XAn_{max} and XAn_{avg} correlate quite well. The key observations, however, which should be incorporated into any model explaining the petrogenesis of the megacrysts and anorthosite xenoliths, are:

- there are significant differences in XAn_{avg} between various megacrysts in a single dyke;
- the range of X_{An} in any single crystal which has a wavy-oscillatory zonation can be as large as the range in XAn_{avg} of all the crystals in one particular dyke, but the two ranges may be different; and
- with only one exception (GM 1750 f 2), megacrysts from BFD 1 have significantly higher XAn_{avg} and XAn_{max} values than megacrysts from BFD 2 (Fig. 7).

The main features of all megacrysts analysed are summarised in Table 3. The magnitude of the jump in

Table 1. Representative microprobe analyses of plagioclase. *MC* Megacryst

Sample	GM 1680	GM 1680	GM 1680	GM 1680	GM 1681	GM 1682	GM 1682	GM 1729	GM 1729	GM 1729	GM 1750	GM 1755
Fsp. no.	1	6	6	6	1	3	4	3	4	5	1	1
	Matrix	MC rim	MC rim	MC core	MC core	MC core	MC core	Matrix	MC core	MC core	MC core	MC core
SiO_2	54.50	54.20	53.75	56.22	55.82	56.49	55.70	58.70	54.64	55.16	58.13	58.59
TiO_2	0.14	0.08	0.09	0.03	0.17	0.15	0.15	0.10	0.03	0.13	0.10	0.08
Al_2O_3	28.16	28.35	28.93	26.55	27.39	26.65	26.55	24.82	27.52	27.01	25.34	25.19
FeO	0.59	0.43	0.38	0.43	0.30	0.47	0.53	0.48	0.55	0.60	0.46	0.53
MnO	0.01	0.01	0.00	0.03	0.00	0.00	0.00	0.00	0.00	0.01	0.01	0.01
MgO	0.08	0.08	0.08	0.08	0.08	0.08	0.07	0.05	0.07	0.06	0.07	0.06
BaO	0.33	0.26	0.28	0.29	0.00	0.08	0.09	0.17	0.00	0.10	0.28	0.27
SrO	0.07	0.00	0.03	0.00	0.26	0.28	0.31	0.25	0.28	0.31	0.02	0.11
CaO	11.49	11.91	12.22	10.09	10.51	9.56	9.75	7.40	10.54	10.17	8.45	8.03
Na_2O	4.76	4.61	4.20	5.44	5.13	5.54	5.51	6.62	5.01	5.26	6.15	5.99
K_2O	0.37	0.33	0.27	0.62	0.41	0.61	0.59	0.95	0.59	0.59	0.95	1.15
Total	100.50	100.26	100.22	99.78	100.08	99.91	99.25	99.54	99.23	99.40	99.96	100.02
Formulae based on 8 oxygens												
Si	2.46	2.45	2.43	2.55	2.52	2.55	2.54	2.65	2.49	2.52	2.62	2.64
Ti	0.00	0.00	0.00	0.00	0.01	0.01	0.01	0.00	0.00	0.00	0.00	0.00
Al	1.50	1.51	1.54	1.42	1.46	1.42	1.43	1.32	1.48	1.45	1.35	1.34
Fe^{2+}	0.02	0.02	0.01	0.02	0.01	0.02	0.02	0.02	0.02	0.02	0.02	0.02
Mn	0.00	0.00	0.00	0.00	0.00	0.00	0.00	0.00	0.00	0.00	0.00	0.00
Mg	0.01	0.01	0.01	0.01	0.01	0.01	0.00	0.00	0.00	0.00	0.01	0.00
Ba	0.00	0.00	0.00	0.00	0.00	0.00	0.00	0.00	0.00	0.00	0.01	0.01
Sr	0.01	0.01	0.01	0.01	0.01	0.01	0.01	0.01	0.01	0.01	0.00	0.00
Ca	0.56	0.58	0.59	0.49	0.51	0.46	0.48	0.36	0.52	0.50	0.41	0.39
Na	0.42	0.40	0.37	0.48	0.45	0.49	0.49	0.58	0.44	0.47	0.54	0.52
K	0.02	0.02	0.02	0.04	0.02	0.04	0.03	0.05	0.03	0.03	0.05	0.07
Total	5.00	5.00	4.98	5.00	4.98	4.99	5.00	5.00	5.00	5.00	5.00	4.99
X_{An}	0.56	0.58	0.61	0.49	0.52	0.47	0.48	0.36	0.52	0.50	0.41	0.41
X_{Ab}	0.42	0.40	0.38	0.48	0.46	0.49	0.49	0.58	0.45	0.47	0.54	0.54
X_{Or}	0.02	0.02	0.02	0.04	0.02	0.04	0.03	0.06	0.03	0.03	0.05	0.05

X_{An} at the core-rim boundary is quite variable and some megacrysts do not show a distinct rim at all. Megacrysts with lower X_{An} in the core also have lower X_{An} in the rim. None of the megacryst rims from BFD 2 crystals reach values of X_{An} ~0.6 which are typically observed in BFD 1 megacrysts and matrix plagioclases.

Strontium isotopic zoning in plagioclase

One megacryst (GM 1680 f 6) was selected for Sr isotopic analysis (Fig. 8, Table 4). Based on the initial $^{87}Sr/^{86}Sr$ ratios, one can distinguish between an inner core (points 1 and 2) with a relatively high Sr_i of 0.7044, and an outer core (points 3–6) with Sr_i values between 0.7036 and 0.7039 (Fig. 9). The decrease in Sr_i from inner to outer core ($\Delta Sr_i = 0.0005$) appears to be quite sharp and is outside analytical uncertainty. The Sr_i isotopic composition within the outer core remains constant within analytical uncertainty, and the rim is very similar to the outer core in terms of its Sr_i composition of 0.7037 (Table 4, Fig. 9). However, there is a difference in the $^{87}Rb/^{86}Sr$ ratio of more than one order of magnitude between the rim analysis and all the core analyses. Overall, the data reveal significant within-core isotopic compositional variations but these variations are not related to the core-rim boundary determined by microprobe.

$^{87}Sr/^{86}Sr$ initial ratios of BFDs in the Isortoq region, determined on clinopyroxene separates, vary between 0.7030 and 0.7038 at 1.19 Ga (Halama, unpublished data). Thus, the Sr initial ratios of clinopyroxenes from BFDs overlap with values from both megacryst rim and outer core but are considerably smaller than values from the inner core (Fig. 9).

Trace-element concentrations

Representative trace-element compositions of six plagioclase cores from four different BFD 1 samples are shown in Table 5. The comparison focuses on two main aspects: firstly, the variation of trace-element contents with X_{An} of the plagioclases (Fig. 10) and secondly, inter-trace-element variations (Fig. 11). In general, there is no correlation between trace-element content and X_{An} in individual crystals and between samples. Trace-element contents of Ba, Ga and Ce (Fig. 10) and Sr, Y, La and Nd (not shown) are variable but apparently independent of X_{An}. The relatively large spread can be attributed mainly to differences in trace-element concentrations between individual crystals with similar An contents, especially for $X_{An} > 0.5$. Many of the trace elements measured in the megacryst cores show a positive correlation, e.g. Sr–Ba, Sr–Ga, Sr–Y, Sr–REEs, Ba–Ga and Ba–REEs. Accordingly, ratios of various trace elements are relatively constant (Fig. 11).

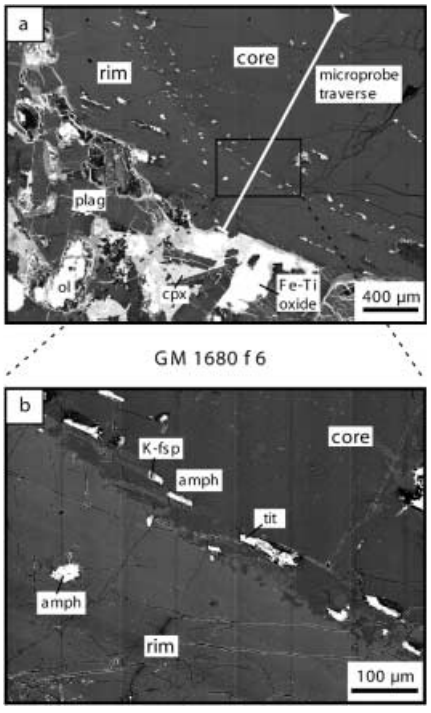

Fig. 6a, b. Back-scattered electron images from the core-rim boundary of the analysed megacryst GM 1680 f 6. **a** Overview, with various matrix minerals in the lower left corner (*ol* olivine, *cpx* clinopyroxene, *plag* plagioclase). The core-rim boundary is marked by a colour difference in the BSE image and a trail of relatively light inclusions. The microprobe traverse extends for further 2,200 µm into the core of the crystal. **b** Details of the core-rim boundary. Note the various embayments and laths of rim-plagioclase within the core and the concentration of inclusions at the boundary (*amph* amphibole, *tit* titanite)

Table 2. Comparison of matrix plagioclase and megacryst rim compositions

Sample	Component	An_{max}	An_{min}
GM 1680	Matrix plagioclase	$An_{55}Ab_{43}Or_2$	$An_{37}Ab_{61}Or_2$
	Megacryst rim	$An_{62}Ab_{37}Or_1$	$An_{37}Ab_{59}Or_4$
GM 1729	Matrix plagioclase	$An_{59}Ab_{39}Or_2$	$An_{32}Ab_{66}Or_2$
	Megacryst rim	$An_{58}Ab_{41}Or_1$	$An_{29}Ab_{68}Or_3$
GM 1750	Matrix plagioclase	$An_{48}Ab_{48}Or_4$	$An_{19}Ab_{69}Or_{12}$
	Megacryst rim	$An_{53}Ab_{44}Or_3$	$An_{37}Ab_{59}Or_4$

Calculation of parental-melt composition

In addition to the measurements from various crystal cores dealt with above, one trace-element profile was obtained across megacryst f 6 from sample GM 1680 (Fig. 12). To investigate the processes which contributed to the sharp discontinuity between core and rim, trace-element concentrations in the crystal were recalculated to concentrations in the original melt, using partition coefficients between plagioclase and melt for the respective element determined by Bindeman et al. (1998). Partition coefficients between plagioclase and melt for various elements have been published also by Simmons and Hanson (1978), Morse (1988), Blundy and Wood (1991), and Vander Auwera et al. (2000), but the data

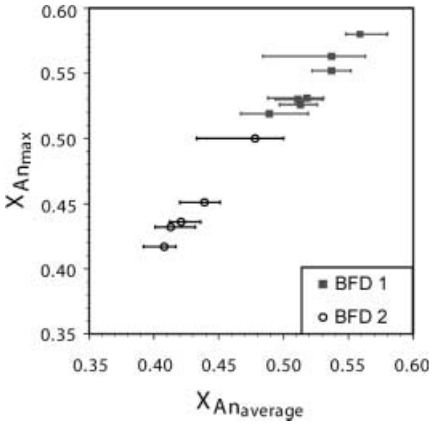

Fig. 7. Comparison of X_{An} values from the cores of various megacrysts in BFD 1 and 2. The *circles*/*squares* show the average core composition and the error bars indicate the maximum and minimum X_{An} values found in the respective cores

from Bindeman et al. (1998) were chosen in this study because they provide a consistent data set for the elements analysed (Table 6).

Trace-element incorporation into plagioclase depends, among other things, on the major-element crystal chemistry. Since core and rim of the megacryst show considerable differences in X_{An}, measured trace-element concentrations partly reflect the major-element crystal composition and not necessarily differences in the melt from which they crystallised. Therefore, the recalculation of the trace-element contents in the melt allows us to constrain chemical differences in the melt much better than does a comparison of the measured concentrations in the crystal.

The distribution of trace elements between crystal and coexisting melt is given by the partition coefficient D_i which is defined as D_i = concentration of element i in crystal/concentration of element i in melt. Partition coefficients may vary with pressure, temperature, composition of the melt and crystal composition (Blundy and Wood 1991). For plagioclase, crystal composition (represented by mol% An) is considered to be the most important parameter in controlling D_i (Blundy and Wood 1991). According to Bindeman et al. (1998), partition coefficients between plagioclase ($0.4 < X_{An} < 0.8$) and melt can be expressed by the general formula

$$RT \ln D_i = a_i X_{An} + b_i,$$

where R is the gas constant, T is the temperature (K), and a_i and b_i are constants determined experimentally specific to each element (Bindeman et al. 1998).

In their partition experiments, Bindeman et al. (1998) used a basaltic melt chemically similar to the gabbroic dykes investigated in this study, and therefore their D_i values can be used here with confidence. X_{An} at the laser spots was measured by EMP and then used for the calculations of the D_i values. We performed our calculations at constant P and T because the pressure

Table 3. Key features of all megacrysts analysed. *Osc*. Oscillating, *Const*. constant, *X* not described accurately due to large step size

BFD no.	Sample	Step size (μm)	Profile length (μm)	No. of analyses (total/core)	Core An_{max}	Core An_{min}	Core $An_{avg} \pm 1\sigma$	$\Delta An = An_{core} - An_{rim}$ (mol%)	Major-element pattern (core)	Core-rim transition
1	GM 1680 f 6	20	3,820	192/160	51.0	46.4	48.9 ± 1.2	+11.0	Osc.	Sudden
1	GM 1681 f 1	500	16,500	34/34	55.2	52.2	53.7 ± 0.8	–	Osc.	–
1	GM 1682 f 2	50	600	13/6	51.6	50.5	51.2 ± 0.7	+5.2	Const.	X
1	GM 1682 f 3	20	3,460	174/152	53.1	48.8	51.8 ± 0.9	+4.8	Const.	Smooth
1	GM 1699 f 1	500	13,500	28/27	58.0	54.8	55.9 ± 0.6	+5.6	Const.	X
1	GM 1729 f 1	100	1,400	15/11	53.6	51.6	52.5 ± 0.6	+8.7	Const.	X
1	GM 1729 f 4	10	2,290	230/199	56.3	48.4	53.7 ± 2.0	+7.9	Const. + Osc.	Sudden
1	GM 1729 f 5	10	430	44/33	53.0	49.4	51.1 ± 1.2	+5.3	Const. + Osc.	Sudden
1	GM 1733 f 1	500	22,000	45/45	52.6	49.7	51.3 ± 0.8	–	Const.	–
2	GM 1750 f 1	10	810	82/69	43.2	40.1	41.3 ± 0.6	+9.2	Const.	Sudden
2	GM 1750 f 7	20	980	50/47	50.0	43.3	47.8 ± 1.3	–	Osc.	–
2	GM 1753 f 7	10	430	44/43	45.1	42.0	43.9 ± 0.5	–9.8	Const.	Sudden
2	GM 1755 f 1	10	760	77/56	41.7	39.2	40.8 ± 0.6	+9.0	Const.	Inhomogeneous
2	GM 1755 f 2	10	370	38/35	43.6	41.2	42.1 ± 0.5	+3.3	Const.	Sudden

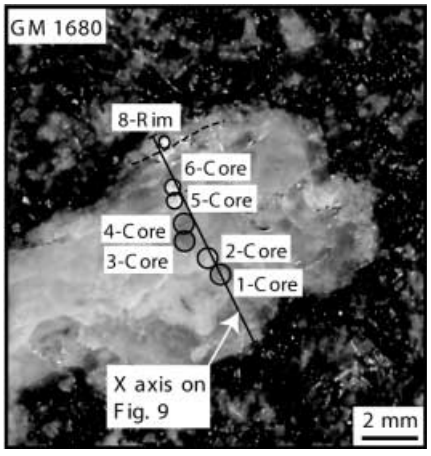

Fig. 8. Photographic image of megacryst GM 1680 f 6, showing the location of the Sr isotopic composition profile. *Circles* approximate the size of the drill samples collected and sample names correspond to Table 4

dependence of $D_i^{plag-melt}$ values has not been determined for most elements except Sr (Vander Auwera et al. 2000). Sr increase per kbar pressure increase in the calculated melt is less than 1% of the Sr concentration in the melt. Therefore, a correction for pressure variations is considered to be unnecessary in the present study.

The temperature dependence of D_i values is more important and changes in T may produce changes in D_i values. However, magmatic temperature variations of 100 °C produce a smaller than 10% effect on RT $\ln D_i$ values, which is within the natural and analytical dispersion (Bindeman et al. 1998). Quantitative information on the crystallisation temperature for the megacrysts is lacking, but Markl et al. (1998) calculated crystallisation temperatures of 1,100–1,185 °C at pressures between 4 and 9 kbar for anorthosites from the Lofoten Islands. Therefore, a constant temperature of T = 1,150 °C, which is in the middle of the temperature range determined by Markl et al. (1998), has been chosen for our calculations.

The calculated Sr content of the melt from which the megacryst crystallised is very constant at roughly 410 ± 20 ppm (Fig. 12). Sr melt concentrations calculated from megacryst rims are initially higher (460–540 ppm) and decrease as the outermost part of the crystal grew. Calculated Ba contents in the parental melts show fairly constant values during core growth, but slightly lower values with some scatter during crystallisation of the rim. Calculated P, Ce and Nd concentrations in the original melt exhibit a wide range, which leads to a wide overlap between melt compositions calculated from core and rim concentrations. As for the other REEs, calculated La concentrations exhibit a relatively large scatter but rim values are somewhat lower than core values. For Ga, adequately determined partition coefficients are lacking, and therefore Ga concentrations as measured in the crystal were plotted.

Table 4. Isotopic data of drill samples from megacryst GM 1680 f 6

Sample	Rb (ppm)	Sr (ppm)	$^{87}Rb/^{86}Sr$	$^{87}Sr/^{86}Sr$	$(^{87}Sr/^{86}Sr)_i$, T = 1.19 Ga
GM 1680-1-core	0.578	266.37	0.0063	0.704510 ± 34	0.704403
GM 1680-2-core	0.182	130.39	0.0040	0.704485 ± 28	0.704416
GM 1680-3-core	0.239	274.70	0.0025	0.703929 ± 17	0.703886
GM 1680-4-core	0.645	782.24	0.0024	0.703690 ± 20	0.703649
GM 1680-5-core	1.035	1060.58	0.0028	0.703860 ± 27	0.703812
GM 1680-6-core	0.658	331.06	0.0056	0.703910 ± 11	0.703815
GM 1680-8-rim	3.919	97.86	0.1158	0.705684 ± 110	0.703711

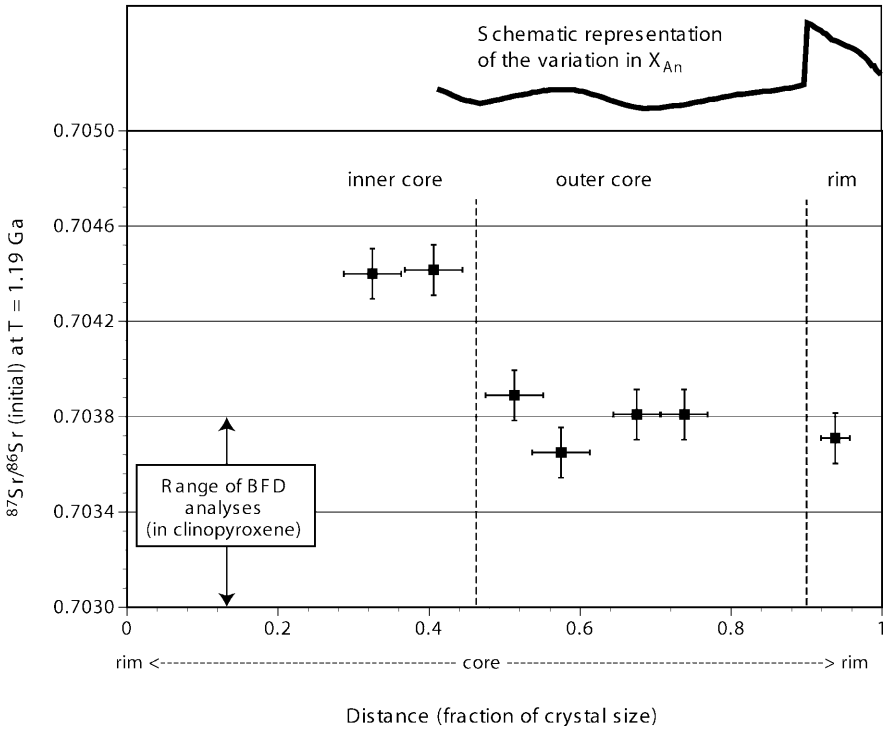

Fig. 9. Sr isotopic composition profile of sample GM 1680 f 6. The rim region is equivalent to the rim detected by microprobe

Ga contents in the rim are about 5–10 ppm lower than in the crystal core.

A comparison of the calculated trace-element concentrations in the melt during rim crystallisation with BFD whole-rock XRF analyses (Halama, unpublished data) shows an overlap for Ba and Sr contents (Table 6). P contents in the calculated melt, however, are significantly above the values determined by XRF.

Discussion

Zoning patterns in plagioclase megacryst cores

Oscillatory zoning in plagioclase is a widespread phenomenon observed in volcanic and subvolcanic environments (e.g. Anderson 1984; Pearce 1994; Kuritani 1998; Ginibre et al. 2002). These zoning patterns are typically characterised by small-scale oscillations ($\leq$ 10 μm) which have been subdivided by Ginibre et al. (2002) into saw-tooth zones with dissolution surfaces (5–10 μm) resulting from magma-chamber dynamics and small-scale oscillations ($\leq$ 1–3 μm) caused by kinetic effects. However, none of those oscillations is comparable to the large-scale, wavy-oscillatory patterns in the cores of a number of megacrysts observed here. Accordingly, none of the numerous theoretical and numerical models developed (e.g. Allègre et al. 1981; Lasaga 1982; L'Heureux and Fowler 1994, 1996) may be applicable to explain these zonations.

As a first step to evaluate the influence of various parameters on the oscillatory zoning, it is important to determine whether the core grew under near-equilibrium or disequilibrium conditions. To assess equilibrium versus non-equilibrium partitioning behaviour, Brophy et al. (1996) compared major- and trace-element abundances of two different crystals from the same sample and concluded from the similar absolute concentrations that partitioning occurred under near-equilibrium conditions. Megacrysts in the BFDs are possibly picked up from different areas in the source volume, so this approach may not give unequivocal results. However, a comparison of two megacrysts from sample GM 1729 yields very similar and constant Fe, Ti, Mg, Ba and Sr concentrations. Molar proportions of An, Ab and Or are also similar and show the same wavy pattern in the core next to the core-rim boundary. The generally smooth megacryst core zoning profiles and the lack of dissolution surfaces within all cores studied (resorption occurs only at the core-rim boundary) are further indications that growth occurred under near-equilibrium conditions.

Under near-equilibrium conditions, small changes in T and water content do not have a major effect on plagioclase composition (Loomis and Welber 1982). The effect of pressure on the zoning patterns can be evaluated using the experimental data from Longhi et al. (1993). The variation of 2–4 mol% An content would correspond to pressure differences of 2–4 kbar or a crustal thickness of roughly 6–12 km. A crystal travelling up and down through a magma reservoir of this depth is geologically unreasonable. Therefore, a change in melt composition remains as a possible factor. Most likely, this change occurs when the crystal is moving around in the magma chamber to compositionally different areas, driven by convective currents (Upton 1996).

Table 5. Representative laser ICP-MS analyses of plagioclase

Sample	GM 1680	GM 1680	GM 1680	GM 1680	GM 1681	GM 1682	GM 1682	GM 1729	GM 1729	GM 1729
Fsp. no.	1	6	6	6	1	3	4	3	4	5
	Matrix	MC rim[a]	MC rim	MC core	MC core	MC core	MC core	Matrix	MC core	MC core
P	Trace	186	Trace	266	123	312	272	267	Trace	392
Sc	Trace	Trace	Trace	27	n.d.	57	50	61	Trace	93
V	3.0	2.1	2.8	2.4	1.7	3.3	2.8	3.3	3.2	4.4
Zn	6.7	8.6	6.2	10.7	Trace	19.6	23.3	17.4	16.4	30.9
Ga	40	35	37	46	24	39	39	40	27	58
Ge	Trace	8	9	11	n.d.	24	27	Trace	n.d.	30
Rb	n.d.	n.d.	n.d.	n.d.	Trace	5.7	5.5	Trace	n.d.	Trace
Sr	1,138	1,277	1,274	1,331	893	1,388	1,356	776	1,112	1,920
Y	0.3	0.2	0.2	0.3	0.3	0.4	0.3	0.2	0.3	0.6
Sn	0.5	1.8	1.9	2.8	2.0	3.5	2.7	1.4	2.1	1.6
Cs	n.d.	n.d.	n.d.	n.d.	n.d.	1.9	Trace	n.d.	n.d.	n.d.
Ba	370	360	367	654	243	624	703	723	445	952
La	2.32	2.03	2.05	3.25	1.18	4.11	3.87	1.75	2.12	6.18
Ce	3.96	3.48	3.45	5.40	2.40	5.94	7.57	2.87	3.78	7.89
Pr	0.38	0.41	0.36	0.51	0.23	0.76	0.80	0.27	0.38	0.81
Nd	1.32	1.58	1.05	1.81	1.01	2.33	3.53	1.02	1.34	3.77
Sm	Trace	n.d.	0.31	0.33	n.d.	n.d.	0.65	n.d.	Trace	0.74
Eu	0.72	0.72	0.86	0.75	0.59	1.14	0.92	1.17	0.58	1.15
Gd	Trace	0.50	n.d.	0.49	Trace	0.92	0.77	0.48	Trace	0.74
Tb	n.d.	n.d.	Trace	0.06	n.d.	0.15	0.13	Trace	n.d.	Trace
Dy	n.d.	Trace	Trace	Trace	Trace	0.71	0.37	Trace	0.35	n.d.
Ho	Trace	0.05	n.d.	Trace	n.d.	0.12	0.13	n.d.	n.d.	Trace
Er	n.d.	Trace	n.d.	n.d.	n.d.	0.63	Trace	Trace	n.d.	Trace
Tm	n.d.	n.d.	n.d.	Trace	n.d.	0.10	n.d.	Trace	n.d.	0.07
Yb	n.d.	n.d.	n.d.	n.d.	n.d.	n.d.	n.d.	n.d.	n.d.	n.d.
Lu	n.d.	n.d.	Trace	n.d.	n.d.	0.14	n.d.	Trace	n.d.	0.06
Pb	n.d.	n.d.	n.d.	Trace	0.53	2.28	2.19	1.26	1.56	2.21

[a]MC, megacryst; n.d., not detected; trace, concentration is between lower limit of decision (2 standard deviations above background) and lower limit of detection (3.28 standard deviations above background)

Phenocrysts in the magma can avoid capture by the advancing solidification front through floating or settling (Marsh 1996). The smooth changes in X_{An} indicate a rather slow and non-turbulent motion. Mechanisms thought to cause repeated compositional changes in the environment of a growing crystal include magma replenishment (Marsh 1996) and movement of the crystal along thermal and compositional gradients (Marsh 1989). The concept of gradual magma mixing is in accordance with the available data. It can explain wavy-oscillatory major-element zonation and is consistent with some variation in the trace-element contents. If the mixing process is slow, resorption surfaces are not likely to develop.

Given their slow isotopic equilibration rates with respect to Sr, plagioclase crystals should retain magmatic Sr isotopic compositions and are therefore useful as recorders of changing isotopic composition in a magma (Cherniak and Watson 1992; Giletti and Casserly 1994). Therefore, it can be assumed that the Sr isotopic ratios of the plagioclase crystals reflect isotopic ratios in the magma. The variation of the initial $^{87}Sr/^{86}Sr$ ratios within the megacryst core of GM 1680 is consistent with an initially xenocrystic or mixing origin early in its crystallisation history. The high $(^{87}Sr/^{86}Sr)_i$ part of the crystal may have been derived from a lower crustal country rock, but the smooth major-element profiles and the petrographic observations do not support such an origin. Hence, an origin involving the assimilation of crustal material is more likely and consistent with the concept of gradual magma mixing. The plagioclase crystal could initially have crystallised in a magma severely contaminated by crustal melts, for example, at the wall of the magma chamber or in a first magma batch which reacted with the country rocks. Later, when the crystal was detached from the magma-chamber wall or when the magma conduit was sealed off from the surrounding crustal rocks, it was incorporated into magma with a less radiogenic, initial Sr ratio.

In summary, the zoning patterns in the megacryst cores are thought to be related to movement of particular crystals within a magma reservoir where they encountered melt of variable composition. Those megacryst cores with ± constant X_{An} indicate stable physicochemical conditions during growth.

Significance of the core-rim boundary in plagioclase megacrysts

The core-rim boundary in the plagioclase megacrysts represents a major resorption surface and is characterised by a sudden increase in X_{An} and a concentration of inclusions (Fig. 6). Major resorption surfaces with abrupt changes in anorthite content are generally attributed to changes in P, T, melt composition or water

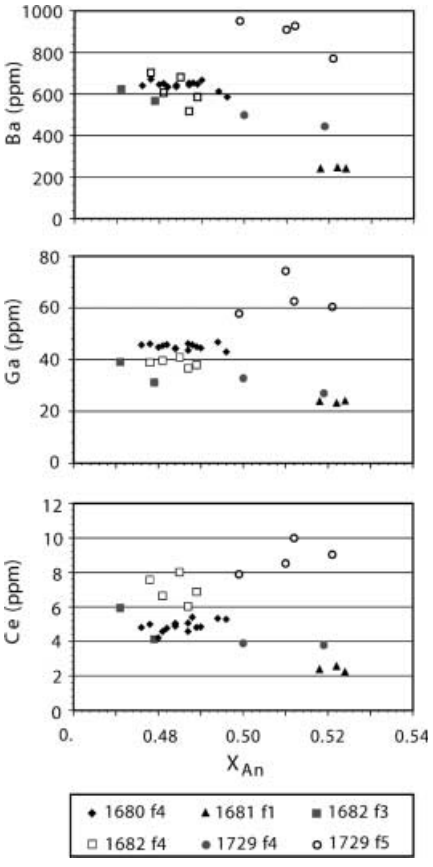

Fig. 10. Plots of Ba, Ga and Ce contents vs. X_{An} in plagioclase from various megacrysts. Trace-element concentrations are apparently unrelated to the major-element composition of the crystal

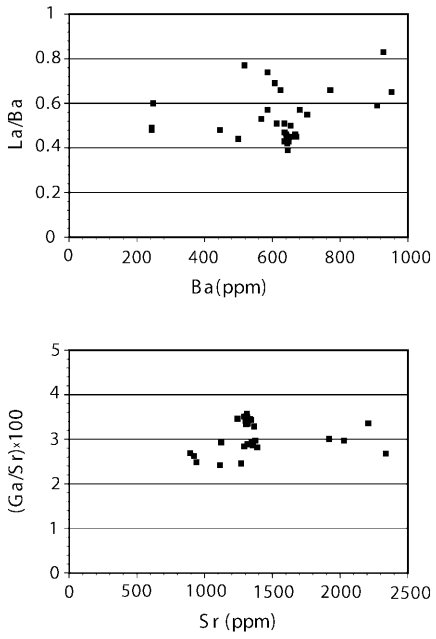

Fig. 11. Plots of La/Ba vs. Ba and Ga/Sr vs. Sr from various megacrysts of BFD 1. Trace-element ratios are relatively constant throughout the range of trace-element concentrations

content of the magma (Singer et al. 1995; Davidson and Tepley 1997), but the ultimate reason for the resorption may be controversial.

As discussed above, it is likely that megacryst cores grew under near-equilibrium conditions so that changes in water content or temperature should not have large effects on the plagioclase composition (Loomis and Welber 1982). However, a short discussion of the less likely case of disequilibrium growth is included here. During disequilibrium growth, increasing temperature or increasing water content in the melt have been invoked to explain resorption and sharp increases in X_{An} (e.g. Loomis and Welber 1982; Anderson 1984). Components other than H_2O are not considered to play a major role in determining the degree of undercooling and thereby the composition of the crystallising plagioclase (Smith and Brown 1988). A sudden water ingress can be envisaged in a subvolcanic environment, but it is more difficult to reconcile with a magma reservoir in mid- to lower crustal depths or close to the crust-mantle boundary, such as is proposed for anorthosite genesis (Ashwal 1993). Sudden changes in temperature are hard to achieve in large volumes of magma due to the low thermal conductivity (Smith and Brown 1988). Therefore, the bulk of evidence indicates that an increase in H_2O content or temperature were not the major factors for the prominent resorption surface between core and rim, so that melt composition and pressure remain as variables responsible for the increase in X_{An} and the resorption.

With the Sr initial isotopic ratios (Fig. 9) and the trace-element profiles (Fig. 12), it can be checked independently whether a compositional change occurred in the melt between core and rim crystallisation and, if so, of what kind. The initial $^{87}Sr/^{86}Sr$ ratios do not show a significant variation between rim and adjacent core values, indicating that the magmas from which the core and rim of the megacryst crystallised were isotopically similar. However, this would be expected if both magmas were derived from the same type of reservoir. Additionally, if an enriched mantle source is assumed for the Gardar magmas (Upton and Emeleus 1987), contamination by lower crustal material with similar Sr isotopic characteristics may not be detected by the Sr isotopes at all. Although the calculated melt-composition trace-element profiles have considerable scatter, minor differences in Sr, Ba and La concentrations between core and adjacent rim indicate that a small change in melt composition took place between growth of core and rim. The melt from which the rim grew appears to be slightly more primitive with lower concentrations of Ba and La than the melt calculated from the core compositions. The higher Sr concentrations in the melt calculated from the rim are possibly reinforced by the pressure dependence of D_{Sr} (Vander Auwera et al. 2000). D_{Sr} decreases with increasing pressure, which means that calculated Sr contents in the melt increase when assuming higher pressures. For Ga, it is not clear whether the drop of Ga contents in the rim is due to a real change in melt composition or whether it is an artefact of a

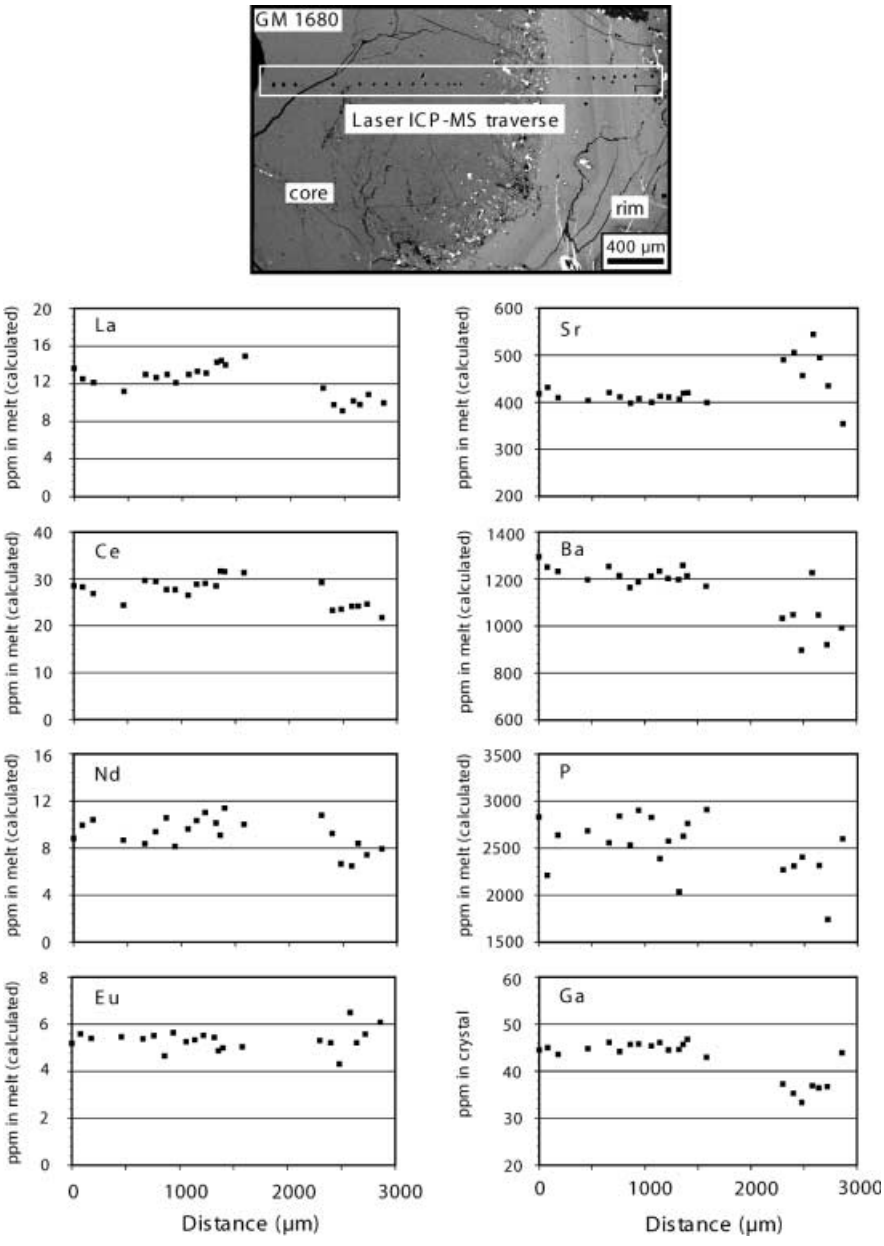

Fig. 12. Laser ICP-MS profile through megacryst GM 1680 f 6. Traverse with 22 spots is shown at the top. Recalculated trace-element concentrations in the melt are shown at the bottom, except for Ga for which the concentrations measured in the crystal are given

supposed change in partition coefficients with crystal chemistry. The overlap of calculated Ce, Nd, Eu and P concentrations between rim and core shows that the compositional change was relatively small. In summary, the compositional change of the magma between core and rim crystallisation is not likely to be responsible for the major resorption surface.

A decrease in pressure has been invoked by Pringle et al. (1974) to explain a sharp boundary between plagioclase core and calcic rim. Subsequent experimental work under anhydrous conditions has shown that there is a general increase in albite content of near-liquidus plagioclase with increasing pressure for a compositional range of starting materials (Greene 1969; Thy 1991; Fram and Longhi 1992; Longhi et al. 1993). Longhi et al. (1993) quantified the shift in plagioclase composition to be ~1 mol% per kbar for anorthosite and somewhat higher for mafic compositions. Decreasing pressure leads to a lowering of the melting temperature of plagioclase in the system An–Ab (Smith and Brown 1988), which in turn leads to resorption of the plagioclase, followed by growth of more An-rich zones under the new pressure conditions. The observed resorption of older plagioclase (core of megacrysts) along cracks and at the former crystal edges is consistent with resorption due to pressure decrease. The concentration of inclusions at, or close to, the core-rim boundary can be explained by a period of rapid crystal growth where melt droplets (now partly recrystallised to secondary minerals) and crystals from the melt have been included.

The megacryst rims with their linear, normal zoning patterns and occasionally superimposed oscillations and

Table 6. Exemplified calculations of partition coefficients and original melt compositions from selected plagioclase analyses

Sample	GM 1680 f 6u	GM 1680 f 6n	GM 1680 f 6h	GM 1680 f 6g	GM 1680 f 6c	Range of melt compositions calculated from the rim	For comparison: range of BFD whole-rock XRF analyses
	Core	Core	Core	Rim	Rim		
X_{An} (mol%)	0.487	0.478	0.496	0.578	0.586		
Trace-element concentrations in the crystal (ppm)							
P	268	248	289	182	182		
Sr	1,305	1,344	1,243	1,235	1,220		
Ba	644	671	586	354	344		
La	2.73	3.02	3.33	2.39	2.01		
Ce	4.58	4.99	5.28	4.36	3.57		
Nd	2.07	2.09	1.97	1.85	1.41		
Eu	0.84	0.84	0.77	0.73	0.71		
Partition coefficients, calculated following the equations from Bindeman et al. (1998) with constant T = 1,150 °C							
D_P	0.10	0.10	0.10	0.08	0.08		
D_{Sr}	3.18	3.26	3.11	2.52	2.46		
D_{Ba}	0.52	0.54	0.50	0.34	0.33		
D_{La}	0.22	0.23	0.22	0.21	0.21		
D_{Ce}	0.17	0.17	0.17	0.15	0.15		
D_{Nd}	0.20	0.20	0.20	0.17	0.17		
D_{Eu}	0.16	0.16	0.15	0.14	0.14		
Trace-element concentrations in the original melt (ppm)							
P	2,639	2,388	2,909	2,271	2,315	1,742–2,599	873–1,026
Sr	410	413	399	490	495	354–544	510–629
Ba	1,232	1,233	1,169	1,033	1,047	897–1,227	750–936
La	12.1	13.3	14.9	11.6	9.8	9.1–11.6	
Ce	26.8	28.8	31.3	29.3	24.2	21.7–29.3	
Nd	10.4	10.4	10.0	10.8	8.4	6.5–10.8	
Eu	5.4	5.3	5.0	5.3	5.2	4.3–6.5	

minor resorption surfaces indicate rapid cooling and simultaneous crystallisation of other phases (Smith and Brown 1988). The rim patterns are comparable to those obtained in experiments (Smith and Lofgren 1983) and numerical simulations (Loomis 1982) with rapid cooling. The similarity of the mineral chemistry between megacryst rims and matrix plagioclases as well as the textural evidence suggest that their crystallisation occurred contemporaneously (Table 2). Kinetically favoured growth on pre-existing plagioclase crystals, where plagioclase could crystallise before matrix crystals started growing, is thought to be the reason that megacryst rims have slightly higher X_{An} values than matrix plagioclase. The overlap of Ba and Sr concentrations of BFD whole-rock XRF analyses with calculated concentrations during rim growth (Fig. 12, Table 6), and the overlap between $^{87}Sr/^{86}Sr$ initial values of the megacryst rim and the BFDs (Fig. 9) also indicate that rim and dyke matrix crystallisation were contemporaneous. The difference in calculated and measured P contents is probably due to the fact that the whole-rock samples do not represent true liquid compositions and some apatite may have been removed by fractional crystallisation. A detailed analysis of the features in the plagioclase rims is beyond the scope of this paper, but it can be concluded that rim growth took place simultaneously with growth of matrix phases at the emplacement level of the dykes.

Following the arguments presented above, an abrupt decrease in pressure as the main reason for the resorption surface is consistent with the available data, possibly accompanied by minor changes in melt composition. Since the increase in X_{An} at the rim occurs in both BFD 1 and BFD 2 megacrysts, it appears that the crystal transport from greater depth to upper crustal levels was a widespread process and the pressure decrease an important factor attending their ascent. The sharpness of the X_{An} increase may indicate that magma ascent was relatively rapid, possibly supported by crack propagation in the crust. Faulting was a significant process in the Gardar events and many dykes inherited their strike direction from earlier structures (Emeleus and Upton 1976). Therefore, it is probable that the magma ascent was associated with tectonic activity, either reactivation of earlier faults or renewed crustal dislocation.

Pressure estimates of megacryst crystallisation

Microprobe profiles with a step size ≤ 20 μm can be taken to yield accurately determined values of $\Delta X_{An}^{core-rim}$. Assuming, for simplicity, that $\Delta X_{An}^{core-rim}$ is caused only by pressure decrease, we can apply the results from Longhi and co-workers to estimate the pressure difference between core and rim growth. $\Delta X_{An}^{core-rim}$ is determined by the adjacent values of X_{An} in the core and in the rim, both of which are variable in the different megacrysts. Assuming that 1-kbar P decrease leads to 1-mol% An increase (Longhi et al. 1993), the maximum $\Delta X_{An}^{core-rim}$ values of 11.0 mol% in BFD 1 and 9.2 mol% in BFD 2

yield maximum pressure differences of 11 and 9 kbar respectively. As the emplacement level of the BFDs is ~1 kbar, the calculations indicate that the megacrysts grew at maximum pressures of 10–12 kbar, which is close to the continental crust-mantle boundary. Lower $\Delta X_{An}^{core-rim}$ values may be explained by crystal growth at higher crustal levels, or by growth in suspensions where the change in X_{An} due to pressure changes can be less pronounced because of a complex interplay of tie-line rotations and mass-balance constraints (Longhi et al. 1993).

Chemical and isotopic constraints on "Big Feldspar Dyke" genesis

The most prominent feature of the BFDs is the variously zoned feldspar megacrysts, and any explanation of BFD genesis must first address the formation of these feldspars and their diversity in X_{An}. Processes contributing to variable plagioclase compositions include

- changes in P and T,
- fractional crystallisation,
- assimilation of crustal material, and
- changes in the degree of partial melting.

Pressure differences may be responsible for variable anorthite contents of megacryst cores, since the albite content of plagioclase increases with increasing pressure (Longhi et al. 1993). This scenario would be in agreement with Marsh's (1996) concept of crystals derived from any depth in the lithosphere – in the case of the plagioclase megacrysts from any crustal depth – which may become entrained and reworked. Taking the two BFDs together, megacryst cores show a compositional difference of 19 mol% An (An_{58} to An_{39}) corresponding to a pressure difference of 19 kbar at constant melt composition. A single magma conduit of such a size is geologically unlikely and it is concluded that pressure differences alone cannot account for the diversity of X_{An} values. However, the entrainment of crystals at various crustal levels may be a viable mechanism in the BFD genesis, and some variation in X_{An} may be attributable to crystallisation at different pressures.

Variations in crystallisation temperature for the various megacrysts are difficult to constrain. Principally, megacryst crystallisation temperatures were probably similar but it appears likely that minor variations in temperature occurred and affected plagioclase chemistry.

Fractional crystallisation during core growth appears not to have occurred on a major scale because of the lack of correlation between incompatible trace-element contents and X_{An} (Fig. 10). If the megacrysts were related to each other by fractional crystallisation processes, one would expect a negative correlation between the contents of incompatible trace elements (e.g. Ba, REEs) and X_{An}, which is not the case. Additionally, the wavy-oscillatory major-element patterns with variably increasing and decreasing X_{An} values indicate that fractional crystallisation did not play a major role during core growth.

As argued above, the variation of the initial $^{87}Sr/^{86}Sr$ ratios within the megacryst core of GM 1680 is consistent with a mixing origin involving the assimilation of crustal material. Interaction of the magma with refractory lower crust is also indicated by the initial ϵ_{Nd} value of –3.7 of BFD 1 derived from the isochron (Halama, unpublished data). It seems likely that the incorporation of chemically diverse crustal material led to variable X_{An} contents, maybe to the degree that the chemistry reflects the degree of mixing between mantle and crust (Dempster et al. 1999). This is in agreement with the trace-element data, since the incompatible trace-element budgets during crust-mantle interaction are likely to be dominated by the crustal source (Bédard 2001) and constant ratios can therefore be expected (Fig. 11). The wide range of trace-element concentrations (Fig. 10) is consistent with variable crustal assimilation as well, but could also have been caused by a variable degree of partial melting.

Summary and conclusions

Petrogenetic model

A preliminary model of BFD petrogenesis is presented below, based on data presented here and also taking into account and combining many ideas of previous workers.

An important aspect of BFD petrogenesis is the intimate relation between megacryst composition and dyke matrix. Bridgwater (1967) noted that X_{An} in megacrysts decreases as the host rocks become more alkaline. This is true for BFD 1 and BFD 2, the former containing high-X_{An} megacrysts and olivine but no quartz whereas the latter bears relatively low-X_{An} megacrysts, no olivine but late interstitial quartz. Bridgwater and Harry (1968) attributed the compositional changes of the dykes to successive tapping of lower levels in a fractionated magma at depth. Marsh (1996) notes that in a rising magma column, magma is flow differentiated and sorted with heavy crystals moving to the centre and downward due to gravity and grain dispersive pressures. Evidence for flow differentiation occurs in many of the dykes where xenoliths and megacrysts are concentrated in the dyke centre (Fig. 3c). Accordingly, BFD 2 could represent a higher part of a solidified magma column than BFD 1. The lighter, relatively Ab-rich megacrysts are therefore predominant in BFD 2 whereas more An-rich, denser megacrysts occur primarily in BFD 1 (Fig. 7).

The generation of the mafic BFD magmas started with minor mantle upwelling (Upton 1996) which supplied heat for melting of lithospheric mantle and/or lower crustal rocks. The maximum pressure derived from the gap in anorthite content at the core-rim

boundary of megacrysts (10–12 kbar) indicates that some megacrysts could have originated at considerable depth. Although there is no independent evidence on the crustal thickness in this region now or in the Proterozoic, it seems a reasonable assumption that 10–12 kbar could correspond to the crust-mantle boundary. Other megacrysts with a less pronounced gap may have crystallised in overlying, lower crustal regions. Some could have grown in a stagnant crystal mush (Wiebe 1992) whereas others moved around in the magma chamber. Because of tectonic stresses acting on the pre-Gardar basement, cracks propagated through the crust and enabled the magmas to rise rapidly.

Although melt composition was crucial in fixing an average X_{An} value in the megacryst cores, sharp changes in X_{An} at the core-rim boundary are independent from core composition. During ascent, megacrysts were probably picked up from various regions of the magma reservoir, possibly throughout the crust which acted as a "gravel pile" of crystals (Marsh 1996). At mid-crustal levels, massif-type anorthositic bodies may have formed (Bridgwater 1967). Single megacrysts and xenoliths derived from the anorthosites were transported in suspension in feldspathic magmas (Scoates 2000) and redistributed after they stopped growing (Winther 1992). Upon emplacement, flow differentiation led to a concentration of megacrysts mainly in the dyke centres, as can be seen from field evidence (Figs. 2, 3).

Bearing on massif-type anorthosite petrogenesis

Since the BFDs are intimately related to Proterozoic massif-type anorthosites (Bridgwater 1967), their occurrence in the Gardar Province and their genesis is thought to hold clues to the formation of anorthositic plutonic complexes in general. The anorthite content in BFD megacrysts is variable but within the range typical of massif-type anorthosites. The occurrence of anorthosite xenoliths in the BFDs implies that MTAs could have formed at depth, although these complexes remain unexposed in the Isortoq region. However, in pre-Atlantic plate-tectonic reconstructions, the Gardar Province is a continuation of the Canadian Shield which contains huge amounts of MTAs of 1.0–1.4 Ga age (e.g. Higgins and van Breemen 1992; Owens et al. 1994). They were emplaced at pressures between 3 and 5 kbar (Fuhrmann et al. 1988; Kolker and Lindsley 1989). The Gardar BFDs, emplaced at roughly 1 kbar, are therefore interpreted to represent a higher crustal level above MTA plutons comparable to the Canadian anorthosites. Our investigations and results offer a unique view upon MTA genesis from a crustal level above these complexes, and can be compared with previously proposed models for their petrogenesis.

Ashwal (1993) proposed a two-stage model of MTA genesis based on the work of many earlier authors (e.g. Bowen 1917; Emslie 1978). In this model, mantle-derived mafic melts are ponded at the crust-mantle boundary, where mafic silicates crystallise and sink and the residual melts become enriched in aluminium. When plagioclase crystallises, it floats and forms anorthositic cumulates at the top of the magma chamber. Gravitationally unstable, plagioclase-rich mushes rise through the crust and form anorthositic massifs in the upper crust. During all stages, heat from the crystallising magmas causes crustal anatexis.

The large-scale major-element oscillatory patterns in plagioclase megacrysts, to our knowledge not described from anywhere else, are thought to be related to movements of the crystals in compositionally diverse magma reservoirs. These magma chambers can be envisaged both at the crust-mantle boundary and/or within the crust. The trace-element and Sr isotope data show that a crustal contribution to the anorthositic magmas was probably important. In accordance with Ashwal's model, crustal contamination is likely in various stages of the magma ascent and could have taken place both by infiltration of crustal melts and by direct assimilation of country rocks (Ashwal 1993).

The major resorption surfaces combined with increases of X_{An} reaching 11 mol% are attributed to a sudden pressure release of up to 11 kbar. This fairly crude estimate of pressure decrease in the plagioclase megacrysts yields crystallisation pressures close to the continental crust-mantle boundary, which is considered to be the site where plagioclase first starts to crystallise in the MTA model (Emslie 1978; Ashwal 1993). Some of the megacrysts from the Gardar Province may represent an initial crystallisation at or near the crust-mantle boundary whereas others may have crystallised during magma ascent. Therefore, our data support the view that the initial crystallisation of MTAs could have started at roughly 30–35 km depth.

The sharp increase in X_{An} at the core-rim resorption surface in the megacrysts also indicates a relatively rapid magma ascent from close to the crust-mantle boundary to the upper crustal levels. Magma batches with entrapped megacrysts must have been able to travel through the crust without being trapped in anorthositic massifs. This seems to be inconsistent with Ashwal's model but it may be explained by the tectonic environment of the Gardar Rift Province, in which extensional stresses and the development of cracks could have facilitated magma ascent during rifting periods when the BFDs were emplaced. In tectonically quieter times, plagioclase mushes could have formed and ascended more slowly to mid-crustal levels (~9–15 km depths) below the BFD emplacement levels, where we would expect to find MTA bodies like those present in Canada. Remnants of both processes can be found today in the "Big Feldspar Dykes" – they contain both single plagioclase megacrysts and anorthosite xenoliths derived from massif plutonic masses.

In the Gardar Province, the BFDs are associated with a variety of other alkaline igneous rocks, including carbonatites (Grønnedal-Ika), agpaitic rocks

(Ilímaussaq) and peralkaline granites (Puklen; Upton and Emeleus 1987). The same is true for the Canadian Shield where occurrences of mid-Proterozoic alkali granites (Strange Lake Complex, e.g. Boily and Williams-Jones 1994), agpaitic alkalic rocks (Red Wine Intrusion, e.g. Curtis and Gittins 1979), syenites (Kipawa Complex, e.g. Currie and van Breemen 1996) and carbonatites (Seabrook Lake Carbonatite, e.g. Cullers and Medaris 1977) have been reported. Given this similarity between Gardar and Canadian rocks, it is tempting to speculate whether this association of alkaline igneous rocks is typical for certain MTA provinces in general. Many geochemical features considered to be characteristic for granitoids associated with MTAs (cf. high Na + K contents, high Fe/Mg ratios, high REE and halogen contents, very Fe-rich mafic silicates; Ashwal 1993) are strikingly similar to those exhibited by the rift-related Gardar rocks.

A plausible model which accounts for the production of a large variety of magmatic rocks in connection with the genesis of massif anorthosites is the "crustal tongue melting model", where underthrusting of a lower crustal mafic tongue is followed by thermal relaxation, asthenospheric uprise and melting of the crustal tongue (Duchesne et al. 1999). In this model, alkaline magmas can be created by contributions from the asthenosphere. Magma uprise takes place along lithospheric discontinuities which could be much older than the anorthosite emplacement (Duchesne et al. 1999). Such structures are present in the Ketilidian Basement of the Gardar rocks (Alaart 1976), and their reactivation during Gardar times makes the model compatible with the well-established rift setting of the Gardar Province (Upton and Emeleus 1987). However, it remains speculative if this model is applicable to the province, and perhaps to the Grenville anorthosites as well.

Acknowledgements We are grateful that we were able to carry out laser ICP-MS measurements at the Large-Scale Geochemical Facility supported by the European Community – Access to Research Infrastructure action of the Improving Human Potential Programme, contract number HPRI-CT-1999-00008 awarded to Prof. B.J. Wood (University of Bristol). B. Paterson provided invaluable help during those measurements. M. Westphal is thanked for his help with the microprobe, and M. Marks for company during fieldwork and many thoughtful comments. Very constructive reviews provided in an exceptionally short time by W. Brown and B. Upton helped to improve the manuscript. Financial funding of this work by the Deutsche Forschungsgemeinschaft (grant Ma-2135/1-2) and the Dansk Grundforskningsfond is gratefully acknowledged.

References

Allaart JH (1976) Ketilidian mobile belt in South Greenland. In: Escher A, Watt WS (eds) Geology of Greenland. Grønlands Geol Undersøg, pp 121–151

Allègre CJ, Provost A, Jaupart C (1981) Oscillatory zoning: a pathological case of crystal growth. Nature 294:223–228

Anderson AT (1984) Probable relations between plagioclase zoning and magma dynamics, Fuego Volcano, Guatemala. Am Mineral 69:660–676

Armstrong JT (1991) Quantitative elemental analysis of individual microparticles with electron beam instruments. In: Heinrich, KFJ, Newbury DE (eds) Electron probe quantitation. Plenum Press, New York, pp 261–315

Ashwal LD (1993) Anorthosites. Springer, Berlin Heidelberg New York

Bédard JH (2001) Parental magmas of the Nain Plutonic Suite anorthosites and mafic cumulates: a trace-element modelling approach. Contrib Mineral Petrol 141:747–771

Bindeman IN, Davis AM, Drake MJ (1998) Ion microprobe study of plagioclase-basalt partition experiments at natural concentration levels of trace-elements. Geochim Cosmochim Acta 62:1175–1193

Bindeman IN, Davis AM, Wickham SM (1999) 400 my of basic magmatism in a single lithospheric block during cratonization: ion microprobe study of plagioclase megacrysts in mafic rocks from Transbaikalia, Russia. J Petrol 40:807–830

Blundy JD, Wood BJ (1991) Crystal-chemical controls on the partitioning of Sr and Ba between plagioclase feldspar, silicate melts, and hydrothermal solutions. Geochim Cosmochim Acta 55:193–209

Boily M, Williams-Jones AE (1994) The role of magmatic and hydrothermal processes in the chemical evolution of the Strange Lake plutonic complex, Quebec-Labrador. Contrib Mineral Petrol 118:33–47

Bowen NL (1917) The problem of the anorthosites. J Geol 25: 209–243

Bridgwater D (1967) Feldspathic inclusions in the Gardar igneous rocks of South Greenland and their relevance to the formation of major anorthosites in the Canadian Shield. Can J Earth Sci 4:995–1014

Bridgwater D, Coe K (1970) The role of stoping in the emplacement of the giant dykes of Isortoq, South Greenland. Geol J Spec Issue 2:67–78

Bridgwater D, Harry WT (1968) Anorthosite xenoliths and plagioclase megacrysts in Precambrian intrusions of South Greenland. Meddr Grønland 185

Brophy JG, Dorais MJ, Donnelly-Nolan J, Singer BS (1996) Plagioclase zonation styles in hornblende gabbro inclusions from Little Glass Mountain, Medicine Lake volcano, California: implications for fractionation mechanisms and the formation of composition gaps. Contrib Mineral Petrol 126:121–136

Cherniak DJ (1995) Diffusion of lead in plagioclase and K-feldspar: an investigation using Rutherford backscattering and resonant nuclear reaction analysis. Contrib Mineral Petrol 120:358–371

Cherniak DJ, Watson EB (1992) A study of Sr diffusion in K-feldspar, Na-K feldspar and anorthite using Rutherford backscattering spectroscopy. Earth Planet Sci Lett 113:411–425

Cullers RL, Medaris G (1977) Rare earth elements in carbonatite and cogenetic alkaline rocks; examples from Seabrook Lake and Callander Bay, Ontario. Contrib Mineral Petrol 65: 143–153

Currie KL, van Breemen O (1996) The origin of rare minerals in the Kipawa Syenite Complex, Western Quebec. Can Mineral 34:435–451

Curtis LW, Gittins J (1979) Aluminous and titaniferous clinopyroxenes from regionally metamorphosed agpaitic rocks in central Labrador. J Petrol 20:165–186

Davidson JP, Tepley FJ (1997) Recharge in volcanic systems: evidence from isotope profiles of phenocrysts. Science 275:826–829

Davidson JP, Tepley FJ, Palazc Z, Meffan-Main S (2001) Magma recharge, contamination and residence times revealed by in situ laser ablation isotopic analysis of feldspar in volcanic rocks. Earth Planet Sci Lett 184:427–442

Dempster TJ, Preston RJ, Bell BR (1999) The origin of Proterozoic massif-type anorthosites: evidence from interactions between crustal xenoliths and basaltic magma. J Geol Soc Lond 156:41–46

Duchesne JC, Liégois JP, Vander Auwera J, Longhi J (1999) The crustal tongue melting model and the origin of massive anorthosites. Terra Nova 11:100–105

Emeleus CH, Upton BGJ (1976) The Gardar period in southern Greenland. In: Escher A, Watt WS (eds) Geology of Greenland. Geological Survey of Greenland, Copenhagen, pp 152–181
Emslie RF (1978) Anorthosite massifs, rapakivi granites, and late Proterozoic rifting of North America. Precambrian Res 7:61–98
Finch AA, Mansfeld J, Andersen T (2001) U-Pb radiometric age of Nunarssuit pegmatite, Greenland: constraints on the timing of Gardar magmatism. Bull Geol Soc Denmark 48:1–7
Fram MS, Longhi J (1992) Phase equilibria of dykes associated with Proterozoic anorthosite complexes. Am Mineral 77:605–616
Fuhrman ML, Frost BR, Lindsley DH (1988) Crystallization conditions of the Sybille Monzosyenite, Laramie Anorthosite Complex, Wyoming. J Petrol 29:699–729
Giletti BJ (1994) Isotopic equilibrium/disequilibrium and diffusion kinetics in feldspars. In: Parsons I (ed) Feldspars and their reactions. Kluwer Academic, Boston, NATO ASI Ser 421, pp 351–382
Giletti BJ, Casserly JED (1994) Strontium diffusion kinetics in plagioclase feldspars. Geochim Cosmochim Acta 58:3758–3793
Giletti BJ, Shanahan TM (1997) Alkali diffusion in plagioclase feldspar. Chem Geol 139:3–20
Ginibre C, Kronz A, Wörner G (2002) High-resolution quantitative imaging of plagioclase composition using accumulated backscattered electron images: new constraints on oscillatory zoning. Contrib Mineral Petrol 142:436–448
Green TH (1969) High-pressure experimental studies on the origin of anorthosites. Can J Earth Sci 6:427–440
Grove TL, Baker MB, Kinzler RJ (1984) Coupled CaAl-NaSi diffusion in plagioclase feldspar: experiments and application to cooling rate speedometry. Geochim Cosmochim Acta 58:2113–2121
Higgins MD, van Breemen O (1992) The age of the Lac-Saint-Jean anorthosite complex and associated mafic rocks, Grenville Province, Canada. Can J Earth Sci 29:1412–1423
Knesel KM, Davidson JP, Duffield WA (1999) Evolution of silicic magma through assimilation and subsequent recharge: evidence from Sr isotopes in sanidine phenocrysts, Taylor Creek Rhyolite, N.M. J Petrol 40:773–786
Kolker A, Lindsley DH (1989) Geochemical evolution of the Maloin Ranch pluton, Laramie Anorthosite Complex, Wyoming: petrology and mixing relations. Am Mineral 74:307–324
Konnerup-Madsen J, Rose-Hansen J (1984) Composition and significance of fluid inclusions in the Ilimaussaq peralkaline granite, South Greenland. Bull Minéral 107:317–326
Kuritani T (1998) Boundary layer crystallization in a basaltic magma chamber: evidence from Rishiri volcano, northern Japan. J Petrol 39:1619–1640
Lasaga AC (1982) Toward a master equation in crystal growth. Am J Sci 282:1264–1288
L'Heureux I, Fowler AD (1994) A nonlinear dynamical model of oscillatory zoning in plagioclase. Am Mineral 79:885–891
L'Heureux I, Fowler AD (1996) Isothermal constitutive undercooling as a model for oscillatory zoning in plagioclase. Can Mineral 34:1137–1147
Longhi J, Fram MS, Vander Auwera J, Montieth JN (1993) Pressure effects, kinetics, and rheology of anorthositic and related magmas. Am Mineral 78:1016–1030
Longhi J, Vander Auwera J, Fram MS, Duchesne J-C (1999) Some phase equilibrium constraints on the origin of Proterozoic (massif) anorthosites and related rocks. J Petrol 40:339–362
Loomis TP (1982) Numerical simulations of crystallization processes of plagioclase in complex melts: the origin of major and oscillatory zoning in plagioclase. Contrib Mineral Petrol 81:219–229
Loomis TP, Welber PW (1982) Crystallization processes in the Rocky Hill Granodiorite Pluton, California: An interpretation based on compositional zoning of plagioclase. Contrib Mineral Petrol 81:230–239
Markl G, Frost BR (1999) The origin of anorthosites and related rocks from the Lofoten Islands, northern Norway. II. Calculation of parental liquid compositions for anorthosites. J Petrol 40:61–77
Markl G, Frost BR, Bucher K (1998) The origin of anorthosites and related rocks from the Lofoten islands, northern Norway. I. Field relations and estimation of intrinsic variables. J Petrol 39:1425–1452
Marsh BD (1989) Magma chambers. Annu Rev Earth Planet Sci 17:439–474
Marsh BD (1996) Solidification fronts and magmatic evolution. Mineral Mag 60:5–40
Mitchell JN, Scoates JS, Frost CD (1995) High-Al gabbros in the Laramie Anorthosite Complex, Wyoming: Implications for the composition of melts parental to Proterozoic anorthosite. Contrib Mineral Petrol 119:166–180
Morse SA (1982) A partisan review of Proterozoic anorthosites. Am Mineral 67:1087–1100
Morse SA (1988) Partition coefficients for anorthosites. Chem Geol 70:154
Owens BE, Dymek RF (2001) Petrogenesis of the Labrieville alkalic anorthosite massif, Grenville Province, Quebec. J Petrol 42:1519–1546
Owens BE, Dymek RF, Tucker RD, Brannon JC, Podosek FA (1994) Age and radiogenic isotopic composition of a late- to post-tectonic anorthosite in the Grenville Province: the Labrieville massif, Quebec. Lithos 31:189–206
Patchett PJ, Bylund G, Upton BGJ (1978) Palaeomagnetism and the Grenville orogeny: new Rb-Sr ages from dolerites in Canada and Greenland. Earth Planet Sci Lett 40:349–364
Pearce TH (1994) Recent work on oscillatory zoning in plagioclase. In: Parsons I (ed) Feldspars and their reactions. Kluwer, Dordrecht, pp 313–349
Pringle GJ, Trembath LT, Pajari GE (1974) Crystallization history of a zoned plagioclase. Mineral Mag 39:867–877
Schiellerup H, Lambert DD, Prestvik T, Robins B, McBride JS, Larsen RB (2000) Re-Os isotopic evidence for a lower crustal origin of massif-type anorthosites. Nature 405:781–784
Scoates JS (2000) The plagioclase-magma density paradox re-examined and the crystallization of Proterozoic anorthosites. J Petrol 41:627–649
Scoates JS, Frost CD (1996) A strontium and neodymium isotopic investigation of the Laramie anorthosites, Wyoming, USA: implications for magma chamber processes and the evolution of magma conduits in Proterozoic anorthosites. Geochim Cosmochim Acta 60:95–107
Simmons EC, Hanson GN (1978) Geochemistry and origin of massif-type anorthosites. Contrib Mineral Petrol 66:119–135
Singer B, Dungan MA, Layne GD (1995) Textures and Sr, Ba, Mg, Fe, K, and Ti compositional profiles in volcanic plagioclase: clues to the dynamics of calc-alkaline magma chambers. Am Mineral 80:776–798
Smith J, Brown WL (1988) Feldspar minerals 1. Crystal structures, physical, chemical and microtextural properties, 2nd edn. Springer, Berlin Heidelberg New York
Smith RK, Lofgren GE (1983) An analytical experimental study of zoning in plagioclase. Lithos 16:153–168
Steiger RH, Jäger E (1977) Subcommission on geochronology: convention of the use of decay constants in geo- and cosmochronology. Earth Planet Sci Lett 36:359–362
Tepley FJ, Davidson JP, Clynne MA (1999) Magmatic interactions as recorded in plagioclase phenocrysts of Chaos Crags, Lassen Volcanic Center, California. J Petrol 40:787–806
Tepley FJ, Davidson JP, Tilling RI, Arth JG (2000) Magma mixing, recharge and eruption histories recorded in plagioclase phenocrysts from El Chicón Volcano, Mexico. J Petrol 41:1397–1411
Thy P (1991) High and low phase equilibria of a mildly alkalic lava from the 1965 Surtsey eruption. Experimental results. Lithos 26:223–243
Upton BGJ (1996) Anorthosites and troctolites of the Gardar Magmatic Province. In: Demaiffe D (ed) Petrology and geochemistry of magmatic suites of rocks in the continental and oceanic crusts. A volume dedicated to Professor Jean Michot,

Université Libre de Bruxelles, Royal Museum for Central Africa, Tervuren, pp 19–34
Upton BGJ, Emeleus CH (1987) Mid-Proterozoic alkaline magmatism in southern Greenland: the Gardar province. In: Fitton JG, Upton BGJ (eds) The alkaline rocks. Blackwell Scientific, Boston, 30, pp 449–471
Vander Auwera J, Longhi J, Duchesne JC (1998) A liquid line of descent of the jotunitic (hypersthene monzodiorite) suite. J Petrol 39:439–468
Vander Auwera J, Longhi J, Duchesne JC (2000) The effect of pressure on D_{Sr} (plag/melt) and D_{Cr} (opx/melt): implications for anorthosite petrogenesis. Earth Planet Sci Lett 178:303–314
Waight TE, Maas R, Nicholls IA (2000) Fingerprinting feldspar phenocrysts using crystal isotopic composition stratigraphy: implications for crystal transfer and magma mingling in S-type granites. Contrib Mineral Petrol 139:227–239
Waight TE, Wiebe RA, Krogstad EJ, Walker RJ (2001) Isotopic responses to basaltic injections into silicic magma chambers: a whole-rock and microsampling study of macrorhythmic units in the Pleasant Bay layered gabbro-diorite complex, Maine, USA. Contrib Mineral Petrol 142:323–335
Waight T, Baker J, Willigers B (2002) Rb isotope dilution analyses by MC-ICPMS using Zr to correct for mass fractionation: towards improved Rb-Sr geochronology? Chem Geol 186:99–116
Wiebe RA (1990) Evidence for unusually feldspathic liquids in the Nain complex, Labrador. Am Mineral 75:1–12
Wiebe RA (1992) Proterozoic anorthosite complexes. In: Condie KC (ed) Proterozoic crustal evolution. Elsevier, Amsterdam, pp 215–261
Winther KT (1992) Feldspar megacryst and anorthosite xenolith-bearing dykes in the Narssarssuaq area, South Greenland. Rapp Grønland Geol Undersøg 154:49–59